

3. These observations are temporarily interpreted in terms of PGMA cross-linking variation basically dependent on the ionization quantity of air caused by electrons ejected from the gold film fabricated on the x-ray mask.

4. In order to suppress electrons ejected from this gold film, a few protective films have been examined. It appears that silicon nitride and Mylar films satisfy the demand.

Acknowledgment

The authors wish to thank Drs. S. Asanabe, K. Ayaki, D. Shinoda, and Y. Okuto for their continuous encouragement.

Manuscript submitted Dec. 27, 1982; revised manuscript received April 21, 1983.

NEC Corporation assisted in meeting publication costs of this article.

REFERENCES

1. J. R. Maldonado, G. A. Coquin, D. Maydan, and S. Somekh, *J. Vac. Sci. Technol.*, **12**, 1329 (1975).
2. Y. Saitoh, H. Yoshihara, and I. Watanabe, *Jpn. J. Appl. Phys.*, **21**, L52 (1982).
3. J. M. Moran and G. N. Taylor, *J. Vac. Sci. Technol.*, **16**, 2020 (1979).
4. K. Okada, *Jpn. J. Appl. Phys.*, **20**, L22 (1981).
5. D. Maydan, G. A. Coquin, J. R. Maldonado, S. Somekh, D. Y. Lou, and G. N. Taylor, *IEEE Trans. Electron Devices*, ed-22, 429 (1975).
6. K. Suzuki and J. Matsui, *J. Vac. Sci. Technol.*, **20**, 191 (1982).
7. H. J. Fitting, *Phys. Status Solidi A*, **26**, 525 (1974).
8. See, for example, H. A. Bethe, "Handbuch der Physik," Vol. 34, S. Flugge, Editor, p. 62, Springer-Verlag, Berlin (1958).
9. See, for example, L. V. Spencer and U. Fano, *ibid.*, p. 121.

Modeling and Analysis of Low Pressure CVD Reactors

K. F. Jensen and D. B. Graves

Department of Chemical Engineering and Materials Science, University of Minnesota, Minneapolis, Minnesota 55455

ABSTRACT

A detailed mathematical model for the hot wall multiple-disk-in-tube LPCVD reactor is developed by using reaction engineering concepts. This model includes the convective and diffusive mass transport in the annular flow region formed by the reactor wall and the edges of the wafers as well as the surface reactions on the reactor wall. In addition, the model describes the coupling of diffusion between and reaction on the wafers. Variations in gas velocities and diffusion fluxes due to net changes in the number of moles in the deposition are also taken into account as are nonisothermal operating conditions. The combined reactor equations are solved by orthogonal collocation. The deposition of polycrystalline Si from SiH₄ is considered as a specific example, and the model is employed in estimation of kinetic rate constants from published reactor measurements. The effects on the growth rates and film thickness uniformity (within each wafer and from wafer to wafer) of variations in flow rates, reactor temperature profiles, and SiH₄ concentration in the feed stream are analyzed. The model predictions show good quantitative agreement with published experimental data from different sources. Finally, recycle of reactor effluent is considered a typical commercial operating conditions, and it is demonstrated that this modification produces higher growth rates and better film uniformity than can be achieved in conventional LPCVD processing.

[001] Chemical vapor deposition (CVD) is a key process in the semiconductor industry for growing thin solid films, in particular polycrystalline Si, Si₃N₄, and SiO₂ films. These materials are grown predominantly in tubular, hot wall, low pressure chemical vapor deposition (LPCVD) reactors which have replaced the earlier cold wall atmospheric pressure reactors. This change has come about because LPCVD reactors allow a larger number of wafers to be processed with better uniformity of film thickness and composition within and among the wafers. Table I gives a summary of LPCVD process conditions for polycrystalline Si, Si₃N₄, and SiO₂. The very large packing densities of wafers that can be realized in LPCVD reactors are possible because at the low process pressures (0.5-1 Torr), the diffusion coefficients are three orders of magnitude larger than at atmospheric pressure so that the chemical reactions at the surface of the wafers are rate controlling rather than mass transfer processes. Moreover, in spite of the low pressures, rates of deposition in LPCVD are only five to ten times less than those obtained in atmospheric CVD since the reactants are used with little or no diluent in LPCVD whereas they are strongly diluted in conventional CVD (1). The wall deposits, which are avoided in cold wall reactors, could create particulate problems in LPCVD processes. However, these potential problems may be avoided by keeping the cumulative wall deposit thin by periodic reactor cleaning.

Key words: LPCVD, polycrystalline Si, modeling, reactors.

The development of CVD reactors and the selection [002] of operating regimes have hitherto mainly been based on empirical design rules. This limits the operation of existing reactors to certain fixed conditions and severely hampers the development of novel deposition processes. Furthermore, the decrease of feature sizes in large scale integrated circuits necessitates the growth of films of highly uniform thickness and composition. This must, of course, be achieved by efficient, economical use of resources. Thus, reaction engineering analysis and design should be a key element in the development and operation of CVD reactors.

CVD in cold wall reactors at atmospheric pressure [003] has been analyzed for two major reactor geometries. Eversteijn *et al.* (2), Rundle (3), and Takahashi *et al.* (4) used various simplifying assumptions to consider the deposition of Si in a horizontal reactor with a flat plate susceptor. Fujii *et al.* (5), Dittman (6), and Manke and Donaghey (7) modeled to various degrees of accuracy the epitaxial growth of Si in a "barrel"

Table I. Typical deposition conditions in LPCVD reactors (1), (21)

Film	Reactant gases	Temperature, °C	Pressure, Torr	Total gas flow, sccm	Dep. rate, Å/min
Poly-Si	SiH ₄	620	0.3	70-100	100-120
	SiH ₄ /N ₂	640	0.5	500-1000	140-160
Si ₃ N ₄	SiH ₄ /NH ₃	800	0.3	100-200	40-60
SiO ₂	SiH ₂ Cl ₂ /N ₂ O	800-900	0.6	200-300	80-120

reactor. None of the investigators took into account that the barrel-formed susceptor may rotate during reactor operation. There have been few and mostly descriptive modeling efforts for LPCVD reactors. Gieske *et al.* (8) and Hitchman *et al.* (9) have presented experimental data and discussed flow fields, mass transfer effects, and possible kinetics but have not formulated a detailed model. Recently, in fact after we had completed this work, Kuiper *et al.* (10) published a model for the LPCVD growth of polycrystalline Si. This simple model omits effects of diffusion in the space between wafers and the significant volume expansion associated with SiH_4 reacting to Si and 2H_2 . Furthermore, the model in its present form is restricted to isothermal conditions and therefore cannot predict reactor temperature profiles that will yield uniform growth rates throughout the reactor. The authors make no attempt to compare the model predictions with experimental observations.

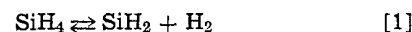
[004] In this paper, we develop a detailed mathematical model for the commercial, multiple-disk-in-tube LPCVD reactor illustrated in Fig. 1. This model includes the physicochemical processes in the annular flow region formed by the tube wall and the edges of the wafers as well as those occurring in the spaces between the wafers. The changes in gas velocity and diffusion fluxes, due to a net production/reduction of mols in the gas phase during the reactions, are taken into account as is the deposition of material on the reactor wall and wafer carrier. A general nonisothermal furnace profile is considered such that variations in growth rates from wafer to wafer may be minimized. We shall demonstrate that the mathematical model correctly predicts experimental observations and gives a quantitative comparison with published experimental data from separate reactor studies. In addition, we shall use the reactor analysis to compare growth rates and thickness uniformities across individual wafers as well as from wafer to wafer for different operating conditions. In particular, the effects of flow rates, diluent (N_2), temperature profiles, and recycle of reactor effluent are elucidated.

Model Development

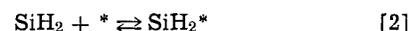
[005] The modeling approach that we present is not restricted to any specific deposition kinetics. However, in order to compare model predictions and experiments, we focus on the low pressure CVD of polycrystalline Si from SiH_4 which is a major LPCVD process for which experimental data have been published. We consider the usual commercial LPCVD re-

actor illustrated in Fig. 1. The wafers are placed perpendicular to main direction of flow and concentrically inside a quartz tube. The flow in the annular region formed by the reactor tube and the wafer edges, *i.e.*, $R_w \leq r \leq R_t$, is laminar. Because of the low pressures, diffusion is the dominant mode of transport in the spaces between the wafers, and the mixing caused by the flow past the wafer edges is negligible. The reactor temperature is controlled by a three-zone heater, and the heats of reaction associated with the deposition are small because of the slow growth rates. Moreover, at the low pressures and high temperatures encountered in LPCVD, heat transfer occurs mainly by radiation. Therefore, we may assume that the temperature profile is determined solely by the furnace settings.

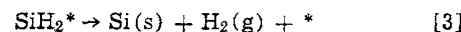
Even though there have been a number of experimental studies of Si deposition from SiH_4 , the kinetic mechanism is not understood (11). It is possible that SiH_4 decomposes in the gas phase (12, 13) according to the reaction



The formed SiH_2 then adsorbs on the Si surface



where it diffuses to a reaction site and decomposes to Si releasing H_2



Since there are no rate data available for the individual reaction steps, we assume, as did Claassen *et al.* (14), that the surface reaction is rate controlling and follows the rate expression

$$\mathcal{R} = \frac{kP_{\text{SiH}_4}}{1 + K_1P_{\text{H}_2} + K_2P_{\text{SiH}_4}} \quad [\text{mol Si}/\text{m}^2 \text{ sec}] \quad [4]$$

This particular form may be justified by the mechanism (Eq. [1]-[3]) and reflects the experimental observations: (i) the rate is inhibited by H_2 , (ii) the rate is first order in SiH_4 at low SiH_4 partial pressures (< 10 m Torr), and (iii) the rate approaches zero order in SiH_4 at high partial pressures (~ 1 Torr) (14). In addition, we may neglect the homogeneous reactions (Eq. [1]) in the ensuing model development and the lumped rate expression (Eq. [4]) used. Considering the lack of detailed kinetic data, the inclusion of the kinetic scheme (Eq. [1]-[3]) in the model would only obscure the reactor analysis.

With the above assumptions and remarks, we are able to construct mathematical models for the stationary operation of the LPCVD reactor shown in Fig. 1. The concentration of the reactant SiH_4 between the wafers is governed by the continuity equation

$$\nabla \cdot N_1 = 0 \quad [5]$$

where N_1 is the molar flux of SiH_4 and

$$N_1 = -\frac{P}{RT} D_{1m} \nabla x_1 + x_1 \sum_{i=1}^3 N_i \quad [6]$$

Here D_{1m} is an effective binary diffusivity and x represents the mol fraction of SiH_4 . The boundary conditions are

$$x_1(r = R_w) = x_{1b} \quad \left. \frac{\partial x_1}{\partial r} \right|_0 = 0 \quad z_1 < z < z_1 + \Delta \quad [6a]$$

$$-N_{1z}|_{\text{wafer } i} = \mathcal{R} \quad N_{1z}|_{\text{wafer } i+1} = \mathcal{R} \quad 0 < r < R_w \quad [6b]$$

where expression [6b] states that the molar flux to the wafer surfaces equals the rate of deposition of Si per unit area. Since the wafer spacing Δ is small compared to the radius of the wafer R_w , *i.e.*, $\Delta/R_w < 0.1$, and the reactant concentration varies smoothly over the length of the reactor, we may neglect the variation in the

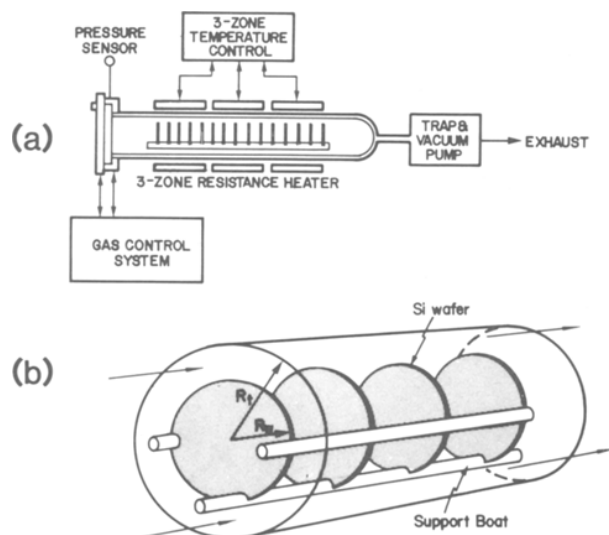


Fig. 1. Schematic of LPCVD reactor: (a) overall system, (b) details of wafer positioning

z-direction within each cell formed by the wafers and use an average SiH_4 concentration. By the averaging process, the boundary conditions (expression [6b]) are incorporated into the continuity balance which now takes the form

$$-\frac{\Delta}{2r} \frac{d}{dr} (rN_1) = \mathcal{R} \quad [7]$$

By using Eq. [6], that $2N_1 = -N_2$ according to the stoichiometry, and that the flux of inerts $N_3 = 0$, the balance takes the form

$$\frac{\Delta}{2r} \frac{P}{RT} D_{1m} \frac{d}{dr} \left(\frac{r}{1+x_1} \frac{dx_1}{dr} \right) = \mathcal{R} \quad [8]$$

with boundary conditions

$$x_1(r = R_w) = x_{1b} \quad \text{and} \quad \left. \frac{dx_1}{dr} \right|_0 = 0 \quad [9a, b]$$

[009] The continuity balance over SiH_4 in the annular flow region has the form

$$\nabla \cdot cD\nabla x_1 - \nabla \cdot (cx_1v) = 0 \quad [10]$$

D is a dispersion coefficient and $D \doteq D_{1m}$ since at low pressures and small Re the mixing occurs mainly by molecular diffusion. The boundary conditions are

$$-D \left. \frac{\partial x_1}{\partial z} \right|_0 = v_0[x_{10} - x_1] \quad [11a]$$

$$R_w < r < R_t$$

$$\left. \frac{\partial x_1}{\partial z} \right|_L = 0 \quad [11b]$$

and

$$-\frac{P}{RT} D \left. \frac{\partial x_1}{\partial r} \right|_{R_t} = \mathcal{R}(R_t) \quad [11c]$$

$$0 < z < L$$

$$\left. \frac{P}{RT} D \frac{\partial x_1}{\partial r} \right|_{R_w} = \left[\frac{R_w}{\Delta} \eta + \alpha \left(\frac{R_t}{R_w} \right) \right] \mathcal{R}(R_w) \quad [11d]$$

[010] Equations [11a] and [11b] are the same as Danckwerts' boundary conditions for fixed bed reactor models. With these boundary conditions, the dispersion model becomes identical to the continuously stirred tank reactor (CSTR) in the limit of very large dispersion coefficients, and it approaches the plug flow reactor (PFR) in the limit of very small dispersion coefficients where convection dominates. The boundary condition (Eq. [11c]) represents the deposition on the hot reactor wall. The first term on the right-hand side of condition (Eq. [11d]) gives the flux of SiH_4 between the wafers due to the deposition of Si. The quantity η is analogous to the effectiveness factor in heterogeneous catalysis (16) and is defined as the ratio of the total rate of reaction on each pair of wafers to that which we would obtain if the concentration were equal to the bulk concentration everywhere in the cell formed by the two wafers, i.e.

$$\eta = \frac{2 \int_0^{R_w} r \mathcal{R}(x_1(r)) dr}{R_w^2 \mathcal{R}(x_1(R_w))} \quad [12]$$

Thus, if the surface reaction is the rate controlling step, $\eta = 1$; whereas if the diffusion between the wafer controls is the rate controlling step, $\eta < 1$. In the limit of strong diffusion resistance, the deposition is confined to a narrow outer band of the wafers and a strongly nonuniform film results. The second term on the right-hand side of Eq. [11d] refers to the deposition on the wafer carrier. α is the area of the carrier relative to reactor tube area.

The pressure drop over the LPCVD reactor is very [011] small (9) so that the total pressure, P , may be considered constant. Therefore, the increase in the number of mols by the deposition reaction $\text{SiH}_4 \rightarrow \text{Si} + 2\text{H}_2$ means an increase in the volumetric flow. To effectively treat this effect, we express the concentration of species in terms of the overall conversion (x) and the fractional change in volume between no conversion and complete conversion (ϵ) (see Ref. (20) for details). The stoichiometry implies that $\epsilon = x_{10}$. The mol fractions of SiH_4 and H_2 are then given by

$$x_1 = \frac{(1-x)x_{10}}{1+\epsilon x} \quad x_2 = \frac{x_{20} + 2xx_{10}}{1+\epsilon x} \quad [13]$$

The gas flow is parallel to the axis of the reactor (the z-direction) and

$$v = v_0(1+\epsilon x)T/T_0 \quad [14]$$

where v_0 is the entrance velocity.

At the low pressures employed in LPCVD, diffusion [012] coefficients are approximately 1000 times larger than those at atmospheric conditions and consequently, the radial mixing is rapid in the annular flow region. Furthermore, the time scale associated with deposition is larger than that for diffusion, i.e., the generalized Damköhler number, $\mathcal{R} \cdot (R_t - R_w)/C_0 D_{1m}$ is small. Therefore, we assume perfect radial mixing and average over the continuity balance by using

$$\langle \cdot \rangle = \frac{\int_0^{2\pi} \int_{R_w}^{R_t} r \cdot dr d\theta}{\int_0^{2\pi} \int_{R_w}^{R_t} r dr d\theta} \quad [15]$$

This averaging eliminates the r -component and includes the boundary conditions Eq. [11c] and [11d] in the one-dimensional continuity balance. Then by making use of the expressions [13] for the mol fractions, the axial velocity (expression [14]), and the temperature dependence of the diffusivity $D/D_0 = (T/T_0)^{1.65}$, we derive the following balance in terms of the conversion, x

$$D_0 \frac{d}{dz} \left(\psi \frac{dx}{dz} \right) + v_0 \frac{dx}{dz} - \frac{2\mathcal{R}}{(R_t^2 - R_w^2) C_{10}} \left[R_t(1+\alpha) + \frac{R_w^2}{\Delta} \eta \right] = 0 \quad [16]$$

where

$$\psi = -\frac{(1+\epsilon)}{(1+\epsilon x)^2} \left(\frac{T}{T_0} \right)^{0.65} \quad [17]$$

The boundary conditions take the form

$$D_0 \left. \frac{dx}{dz} \right|_0 = v_0(1+\epsilon x) \quad \left. \frac{dx}{dz} \right|_L = 0 \quad [18]$$

To set forth the fundamental parameter combinations associated with the deposition process, we make the modeling equations dimensionless by defining

$$Da_1 = \frac{2LR_t(1+\alpha)}{v_0(R_t^2 - R_w^2) C_{10}} \mathcal{R}(x=0)$$

$$Da_2 = \frac{2L R_w^2/\Delta}{v_0(R_t^2 - R_w^2) C_{10}} \mathcal{R}(x=0)$$

$$g(x) = \frac{\mathcal{R}(x)}{\mathcal{R}(x=0)} \quad Pe = \frac{v_0 L}{D_0}$$

$$\xi = \frac{z}{L} \quad \xi = \frac{r}{R_w} \quad \phi^2 = \frac{2R_w^2 \mathcal{R}(x=0)}{\Delta C_{10} D_{1m} (T/T_0)^{0.65}} \quad [19]$$

The reactor Eq. [16] then takes the form

$$\frac{d}{d\xi} \left(\psi \frac{dx}{d\xi} \right) + Pe \frac{dx}{d\xi} - Pe(Da_1 + \eta Da_2)g(x) = 0 \quad [20]$$

with boundary conditions

$$\frac{dx}{d\xi} \Big|_0 = Pe(1 + x(0)\epsilon)x(0) \quad \text{and} \quad \frac{dx}{d\xi} \Big|_1 = 0 \quad [21a, b]$$

and

$$\eta = 2 \int_0^1 \xi \frac{g(x(\xi))}{g(x_b)} d\xi \quad [22]$$

The reaction-diffusion problem governing the wafers becomes

$$\frac{1}{\xi} \frac{d}{d\xi} \left(\frac{\xi}{1 + \epsilon x} \frac{dx}{d\xi} \right) + \Phi^2 g(x(\xi)) = 0 \quad [23]$$

with boundary conditions

$$x(\xi = 1) = x_b(\xi) \quad \text{and} \quad \frac{dx}{d\xi} \Big|_0 = 0 \quad [24a, b]$$

[014] The parameters each have specific physical significances. The Damköhler numbers Da_1 and Da_2 represent the ratios of reactor space time to the characteristic time for deposition on the reactor wall and on the wafers, respectively. The axial Peclet number (Pe) represents the ratio of the time constant for convective transport to that for diffusive transport. The parameter, Φ , is equivalent to the Thiele modulus (ϕ) used extensively in analysis of heterogeneous reactions. It denotes the ratio of the characteristic time for diffusion in between the wafers to the characteristic time for deposition of Si on the wafer surfaces. Thus, if Φ is large, the deposition is hindered by diffusion and a nonuniform film results. This effect is completely analogous to that of a large ϕ for a porous catalyst. In fact, the modeling Eq. [20]-[24] are similar to those for a catalytic fixed bed reactor.

Numerical Solution of the Modeling Equations

[015] The modeling equations form two nonlinear boundary value problems which must be solved by some suitable numerical technique. Here we use the orthogonal collocation method which has been applied successfully to many chemical reaction engineering problems, especially fixed bed reactors [(17), (18) and references therein]. In this method, the first and second spatial derivatives are approximated by a weighted sum of values of the dependent variable at the collocation points

$$\frac{dx}{d\xi} \Big|_{\xi_i} = \sum_{j=0}^{N+1} A_{ij}x_j \quad i = 0, 1, \dots, N + 1 \quad [25]$$

$$\frac{d^2x}{d\xi^2} \Big|_{\xi_i} = \sum_{j=0}^{N+1} B_{ij}x_j \quad i = 0, 1, \dots, N + 1 \quad [26]$$

The weight matrices depend on the trial functions which in our case are the first N Jacobi polynomials $P_i^{(\alpha, \beta)}(\xi)$ with weight function $\xi^\alpha(1 - \xi)^\beta$ (17, ct. 3). Since there is no special symmetry in the tubular reactor problem Eq. [20], we use $(\alpha, \beta) = (0, 0)$ for that equation. However, for the wafer problem (Eq. [23]), advantage is taken of the radial symmetry and the Dirichlet condition (Eq. [24a]) by using $(\alpha, \beta) = (1, 0)$. The collocation points are in each case the zeros of the orthogonal polynomial, $P_N^{(\alpha, \beta)}(\xi)$. By discretizing the reactor Eq. [20], [21], we obtain the following set of nonlinear algebraic equations for the interior

$$\psi_i \sum_{j=0}^{N+1} B_{ij}x_j + \left[Pe + \sum_{j=0}^{N+1} A_{ij}\psi_j \right] \sum_{j=0}^{N+1} A_{ij}x_j = 0 \quad i = 1, \dots, N \quad [27]$$

and for the boundary

$$\sum_{j=0}^{N+1} A_{0j}x_j - Pe(1 + x_0\epsilon)x_0 = 0 \quad [28]$$

$$\sum_{j=0}^{N+1} A_{N+1,j}x_j = 0 \quad [29]$$

In order to solve this system of equations, we [016] need to evaluate $\eta(x_i)$ from the solution to the wafer problem, (Eq. [23]). Since the variations in film thickness across the individual wafers is small (<5%) in most LPCVD reactors, we expect Φ to be small. In that case, it is possible to obtain an accurate solution to the wafer problem by using just one interior collocation point. This technique has been demonstrated to give accurate results for the analogous catalyst particle problem even for moderately large values of Φ (19). Then by using the one-point collocation technique (19), the wafer problem is approximated as

$$\epsilon\Phi^2 g(x(\xi_1)) = 6 \ln \left[\frac{1 + \epsilon x(\xi_1)}{1 + \epsilon x(1)} \right] \quad [30]$$

This equation can be solved for given ϕ^2 , ϵ , and $x(1)$ to yield $x(\xi_1)$. One can then evaluate η_i by Radau quadrature (17, 19) as

$$\eta_i = \frac{2}{g(x(1))} \left[\frac{1}{8} g(x(\xi_1)) + \frac{1}{8} g(x(1)) \right] = \frac{1}{4} \left[1 + 3 \frac{g(x(\xi_1))}{g(x(1))} \right] \quad [31]$$

By combining these equations with the $N + 2$ nonlinear algebraic equations for the reactor tube (Eq. [27]-[29]), we can find the solution to the entire LPCVD problem by Newton-Raphson iteration. This, in turn, enables us to predict growth rates and variations in film thickness within and among wafers. The growth rate on the wall is determined by

$$G_t = \bar{V}_{si}R(x=0)g(x) \quad [32]$$

while the average growth rate on each wafer is

$$\bar{G}_w = \bar{V}_{si}R(x=0)g(x)\eta \quad [33]$$

The average growth rate on all wafers in the reactor is computed by quadratures

$$\bar{G} = \bar{V}_{si}R(x=0) \int_0^1 g(x)\eta d\xi = \bar{V}_{si}R(x=0) \sum_{i=1}^N w_i g(x_i)\eta_i \quad [34]$$

where the w_i 's are Gauss quadrature weights corresponding to the N interior collocation points. The variation in growth rates and thus film thickness is determined as

$$\sigma^2 = \int_0^1 \left[\frac{\bar{G} - \bar{G}_w(\xi)}{\bar{G}} \right]^2 d\xi = \frac{\int_0^1 [g(x)\eta]^2 d\xi}{\left[\int_0^1 g(x)\eta d\xi \right]^2} - 1 \quad [35a]$$

for the reactor

$$\sigma_w^2 = 2 \int_0^1 \xi \left[\frac{G_w - \bar{G}_w}{\bar{G}_w} \right]^2 d\xi = \frac{2}{\eta^2} \int_0^1 \xi \left[\frac{g(x(\xi))}{g(x(1))} \right]^2 d\xi - 1 \quad [35b]$$

within each wafer

These integrals can also be evaluated by quadrature. With the developed mathematical model, we are now able to analyze experimental observations and to draw comparisons between growth rates and possible levels of uniformity at different operating conditions.

Evaluation of Kinetic Parameters

- [017] Since detailed rate data for the pyrolysis of SiH_4 are scarce and often contradictory (11), we chose to evaluate the parameters k , K_1 , and K_2 in expression [4] from experimental data for the deposition of polycrystalline Si in an LPCVD reactor obtained by Claassen *et al.* (14). The reactor was loaded with 50 76.2 mm diam wafers spaced 10 mm apart and it was kept isothermal. Very low concentrations of SiH_4 ($x_{10} = 0.0047$) were used in mixtures of H_2 and N_2 . The relative amount of the carrier gases, H_2 and N_2 , was varied to demonstrate the inhibition of Si deposition by H_2 . Figure 2 shows the experimental data from Claassen *et al.* (14) and the theoretical predicted growth rates as a function of the dimensionless axial reactor position, ξ .
- [018] The model predicts quite well the decrease in growth rates along the reactor length due to depletion of SiH_4 as well as the inhibiting effect of increased H_2 concentration.
- [019] The rate constants determined from this comparison with experimental data are

$$k = 1.25 \cdot 10^9 \exp(-18,500/T) \text{ mol/m}^2/\text{atm}/\text{sec}$$

$$K_1 = 1.75 \cdot 10^3 \text{ atm}^{-1}$$

$$K_2 = 4.00 \cdot 10^4 \text{ atm}^{-1}$$

The activation energy for k is not determined but instead extracted from Bryant's survey of the temperature dependence of Si deposition (11). The "adsorption parameters," K_1 , K_2 , are considered temperature independent in the range of temperatures of interest in LPCVD of polycrystalline Si, 600°-650°C, because of insufficient data. The rate constants were not determined by any statistical technique although the modeling equations could form the basis for non-linear least squares parameter estimation. However, that falls outside the scope of the present work.

- [020] In order to test the ability of our mathematical model to predict growth rates at different conditions than those used in the evaluation of the kinetic parameters, we consider the effect of varying the deposition area by removing wafers. Figure 3 shows mea-

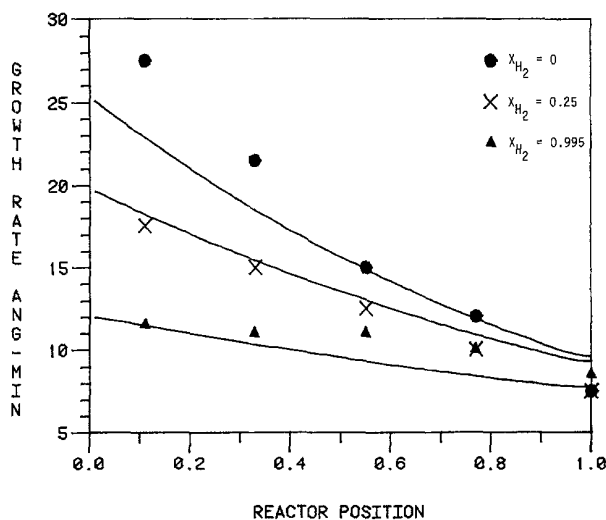


Fig. 2. Model predictions (solid line) vs. experimental data (14) of growth rate profiles as a function of inlet H_2 concentration. Reactor conditions: $P = 0.53$ Torr, $T = 625^\circ\text{C}$, flow = 1000 sccm, $X_{\text{SiH}_4} = 0.0047$.

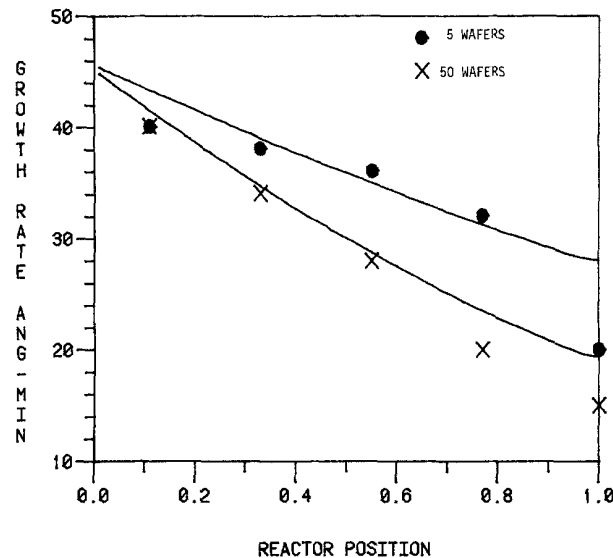


Fig. 3. Model predictions (solid line) vs. experimental data (14) of growth rate profiles as a function of number of wafers in the reactor. Reactor conditions: $P = 0.53$ Torr, $T = 625^\circ\text{C}$, flow = 1000 sccm, $X_{\text{SiH}_4} = 0.0047$.

sured growth rates by Claassen *et al.* (14) and predicted growth rates for the cases of 5 and 50 wafers in a 0.5m reaction zone. The model matches the trend of the experimental observations and demonstrates that, as expected, the growth decreases more rapidly in the case of the larger deposition area (50 wafers) because of the faster depletion of the reactant, SiH_4 . The assumption of a small wafer spacing relative to the wafer radius (i.e., $\Delta/R_t \ll 1$), which was used to eliminate the z -dependence in the wafer problem (Eq. [5], [6]), clearly does not hold for the five-wafer case. This may explain the slightly larger differences between model predictions and experimental observations for the five-wafer run than those for the 50-wafer run.

Comparison of Model Predictions and Commercial Process Data

In order to further test the mathematical model, [021] we consider deposition data obtained by Rosler (1) with a different LPCVD reactor system, and at SiH_4 concentrations two orders of magnitude larger than those used in the above evaluations of the kinetic constants. The same size wafer (76.2 mm diam) was used in the experimental study. The reactor contained 110 wafers spaced at 4.7 mm as well as five dummy wafers at each end of the wafer zone. The possible growth rates and film thickness uniformities for two typical conditions for commercial LPCVD reactors, pure SiH_4 feed and SiH_4 diluted with N_2 , were compared, and the effects of flow rates, reactor temperature profile, and dilution were demonstrated experimentally.

Figure 4 illustrates the measured growth rates (1) [022] and the predicted rates as functions of the wafer position in the reactor for a $\pm 15\%$ change in SiH_4 feed rates around the base case of 47 sccm pure SiH_4 feed. The reactor temperature is varied from 607° to 654°C along the length of the reactor by using the 3-zone furnace to produce a nearly uniform thickness of the polycrystalline Si layer in the base case. The model predictions accurately predict the trends in the experimental data. When the feed rate of SiH_4 is stepped up 15%, the growth rates, as reflected by the Si-thickness, increase along the length of the reactor since there is excess reactant available relative to the base case. A flat thickness profile could clearly be achieved by lowering the temperature gradient along

Explore Litigation Insights

Docket Alarm provides insights to develop a more informed litigation strategy and the peace of mind of knowing you're on top of things.

Real-Time Litigation Alerts



Keep your litigation team up-to-date with **real-time alerts** and advanced team management tools built for the enterprise, all while greatly reducing PACER spend.

Our comprehensive service means we can handle Federal, State, and Administrative courts across the country.

Advanced Docket Research



With over 230 million records, Docket Alarm's cloud-native docket research platform finds what other services can't. Coverage includes Federal, State, plus PTAB, TTAB, ITC and NLRB decisions, all in one place.

Identify arguments that have been successful in the past with full text, pinpoint searching. Link to case law cited within any court document via Fastcase.

Analytics At Your Fingertips



Learn what happened the last time a particular judge, opposing counsel or company faced cases similar to yours.

Advanced out-of-the-box PTAB and TTAB analytics are always at your fingertips.

API

Docket Alarm offers a powerful API (application programming interface) to developers that want to integrate case filings into their apps.

LAW FIRMS

Build custom dashboards for your attorneys and clients with live data direct from the court.

Automate many repetitive legal tasks like conflict checks, document management, and marketing.

FINANCIAL INSTITUTIONS

Litigation and bankruptcy checks for companies and debtors.

E-DISCOVERY AND LEGAL VENDORS

Sync your system to PACER to automate legal marketing.